Science Advances
AAAS

advances.sciencemag.org/cgi/content/full/5/10/eaax0997/DC1

Supplementary Materials for

Earliest occupation of the Central Aegean (Naxos), Greece: Implications for hominin and *Homo sapiens*' behavior and dispersals

Tristan Carter, Daniel A. Contreras, Justin Holcomb, Danica D. Mihailović, Panagiotis Karkanas, Guillaume Guérin, Ninon Taffin, Dimitris Athanasoulis, Christelle Lahaye,

*Corresponding author. Email: stringy@mcmaster.ca (T.C.); christelle.lahaye@u-bordeaux-montaigne.fr (C.L.)

Published 16 October 2019, *Sci. Adv.* **5**, eaax0997 (2018)
DOI: 10.1126/sciadv.aax0997

This PDF file includes:

Supplementary Materials and Methods

1. Luminescence Dating (Continued)

Here we detail some aspects of the analytical procedures relating to luminescence dating.

1.1. Sample preparation and analysis

The 180-250μm (2016 samples) or the 200-250 μm fraction (2017 samples) was isolated by wet-sieving, and treated by hydrochloric acid (10%) and hydrogen peroxide (30%) to remove successively carbonates and organic matter. A density separation (using aqueous solutions of sodium heteropolytungstates) enabled the quartz and feldspar-rich fractions to be isolated. The quartz fraction was then etched with a 40% HF solution for 40 minutes to remove the outer part of the grains affected by external alpha irradiation. The K-feldspar fractions prepared from the 2016 samples were not etched, whereas the 2017 samples received the HF 40% or 10% etching treatment for quartz and feldspar fractions, respectively. All samples were then treated with HCl 10% to remove any fluoride contaminant, and the fractions re-sieved at 180μm (2016 samples) or at 200μm (2017 samples), and rinsed.

Grains were mounted in 9mm diameter stainless steel cups using silicone oil. Aliquots of ~1mm for feldspar extracts and ~5mm for quartz extracts were prepared. The quartz aliquots were measured with a Daybreak 2200 OSL reader (*75*), with Green LEDs (Nichia NSPG 310@515nm, maximum power of 30mW/cm^2). The feldspar aliquots were measured with a Freiberg Instruments *Lexsyg SMART* reader (*76*) for the pIRIR$_{290}$ protocol. The grains were stimulated with near infrared diodes @850nm, and emitted signals were detected with an H7360-02 Photon Counting Head in the UV/Vis region (410 nm) through a combination of optical filters. For IR$_{50}$ measurements, feldspar aliquots were measured with a Risø TL/OSL DA 20

reader (*77*). The grains were stimulated with IR diodes (Vishay TSFF5210) emitting at 870nm. The luminescence signals were detected with an EMI 9235 QA photomultiplier tube (PMT), through a combination of optical filters.

Sub-samples were dried, crushed, compacted, sealed in adapted plastic boxes and stored for at least three weeks. The natural radioelement contents were then measured by high-purity low background Ge gamma spectrometry (*78*).

1.2 Equivalent dose measurements

$pIRIR_{290}$ measurements were performed with a preheat at 320°C for 60s for the natural and regenerated signals, and for the dose tests, and a final bleach at 325°C during 200s to avoid recuperation signals. The test doses were chosen to be ca. 20-25% of the D_e. $pIRIR_{290}$ measurements recycling ratio (*79*) were within 5% of unity, and recuperation ratio were less than 5%, for each aliquot of each sample. $pIRIR_{290}$ curves are provided for sample SNAP17-04 (fig. S5) and show that saturation is far from reached for this sample (the oldest sample of the site, with the highest D_e).

Only the results of the $pIRIR_{290}$ measurements are considered in the discussion, because in each case only a few aliquots (n=3) were measured for IR_{50}. In a first stage, $pIRIR_{290}$ D_e were calculated using the Central Age Model (*74*) and the Average Dose Model (ADM) (*73*) (table S1). The results are very similar, and equal within uncertainties. IR_{50} D_e were calculated without fading correction, and g-values were measured individually, for each aliquot (table S2).

Residual dose measurements were performed, based on two samples (SNAP16-02 and SNAP17-04). The natural signal of both samples was bleached with a Hönle SOL500 solar simulator ($800W.m^{-2}$, 80 cm distance between lamp and sample), during times ranging from 15min to 48h. The remaining doses were then measured, using the same SAR protocol used for $pIRIR_{290}$ D_e determination. As already observed (*80*) no fixed unbleachable residual level is reached, even after 48 hours of bleaching (fig. S6). The remaining dose after 48h is ~ 6-7Gy, representing respectively 5% and less than 1% of the measured D_e values; as a result, and following Kars *et al*. (*80*), we decided not to subtract any residual dose for age calculation (thus, it is possible that

the ages of the four youngest samples – SNAP16-4, SNAP16-3, SNAP16-2 and SNAP16-1 – are slightly overestimated).

In turn, a dose recovery experiment was conducted, by adding a known dose to the natural signal (*60, 81*). Four aliquots of sample SNAP16-03 were measured, after giving a beta dose of 65Gy. After subtracting the natural D_e value, measured for the other 10 aliquots of this sample, the experiment led to a dose recovery ratio of 1.00±0.03. This experiment proves that the parameters chosen to measure the D_e are well-suited for our samples.

1.3 Dose rates

Internal dose rates due to ^{40}K content of the feldspar grains have been calculated assuming a content of 12.5±0.5%, following Huntley and Baril (*82*). The external beta dose rate was calculated from the sediment radioelement contents, measured by HP low background gamma spectrometry (*77*); the results are presented in table S3. The conversion factors were taken from Guérin *et al*. (*83*) and the attenuation factors from Guérin *et al*. (*84*). An alpha efficiency of 0.08±0.02 was assumed for calculating the alpha dose rate (*85*). Water contents have been estimated to 8±6% during burial, based on measurements at the time of sampling. Environmental dose rates (gamma and cosmic contributions) were derived from *in situ* dosimeter measurements. The contributions to the dose rates and the total dose rate for each sample are presented in table S4.

1.4 Ages

A Bayesian model was built with the R 'BayLum' (*86–89*) statistics package, based on $pIRIR_{290}$ ages, taking into account stratigraphic constraints and a covariance matrix of errors (*88, 89*). Models built in 'BayLum' are based on Markov Chain Monte Carlo (MCMC) calculations and allow taking into account the stratigraphic order of samples, as well as the specificities of measurements leading to IRSL ages; therefore, even though the ages thus obtained only slightly differ from those obtained with the ADM, we consider the ages calculated with BayLum as the most representative of sediment deposition at the site. 'BayLum' was run with stratigraphic constraints between all samples; the dose covariance matrix allowed taking systematic errors on the following parameters:

- equivalent dose measurements (a 2% uncertainty was considered on the laboratory source dose rate);
- radioelement concentrations (1%, 0.7% and 0.6% on the concentrations of K, U and Th, respectively, corresponding to the uncertainties on radioelement concentrations on the calibration standard;
- internal dose rate (an uncertainty of 0.03 $Gy.ka^{-1}$ was assumed);
- water concentration; we used a water concentration of 8 ± 6% and considered that the corresponding uncertainty corresponds to a systematic error.

All other sources of errors in the age calculation were treated as random in the Bayesian modelling. The distribution of equivalent doses around the central dose of each sample was modelled by a Gaussian distribution. A good convergence of the Markov Chains was obtained, as can be seen on fig. S8, after 50,000 iterations. The convergence was further confirmed by the Gelman and Rubin indexes, with values below 1.05 (see Philippe *et al*. (*89*), for details on computational aspects). Fig. S9 is a bivariate scatter plot of a sample of observations from the joint posterior distribution of the IRSL ages generated by Markov Chain Monte Carlo calculations, using the 'BayLum' R package. This plot allows visualizing in particular the effect of the stratigraphic constraint between samples SNAP16-4 and SNAP16-3, SNAP16-3 and SNAP16-2, and – although to a lesser degree – SNAP16-2 and SNAP16-1 (see the truncation in the upper-left hand corner of the corresponding panels).

2. Thin-Section Soil Micromorphology

Random and targeted sampling strategies included taking random peds from specific deposits, as well as taking undisturbed blocks using plaster of Paris. Samples were prepared and analyzed at the Malcolm H. Weiner Laboratory for Archaeological Science housed at the American School of Classical Studies at Athens.

Samples were dried at $50^{o}C$ for four days in an oven and impregnated with a mixture of unsaturated resin, styrene, and hardener in a ratio of 7:3:0.012. After three weeks of curation and hardening, samples were cut into 7 cm × 5 cm × 1 cm slabs using a Struers Accutom-2 trim saw. Cut samples (chips) were sent to Quality Thin Sections in Tucson, Arizona where they were prepared as glass slide thin sections.

For thin-section analysis, including pedological and sedimentological interpretation we utilized a Leica DM2700P polarizing light microscope equipped with a digital camera for petrographic analysis at total magnifications 12.5X to 500X using both cross polarized light (XPL) and plane polarized light (PPL). Thin sections were described according to the work of Courty *et al*. (*90*) and Stoops (*91*), with specific references drawn from Stoops *et* al (*92*).

3. Stratigraphy

Here, we describe each Lithostratigraphic Unit [LU] represented in trench DG-A/001 (Fig. 2 and fig. S1); each contained cultural material, with the exception of LU8.

3.1 Lithostratigraphic Unit 1 – Late Pleistocene to Holocene Debris Flow (Soil 1).

Poorly sorted light brown (7.5YR 6/4) silt loam with many sub-angular to angular cobbles throughout. Deposit is matrix supported, soft, and has weak subangular blocky structure with a gradual smooth lower boundary. Deposit has medium to fine pores with common coarse and fine roots throughout. The first ~5-10 cm is marked by a modern soil, characterized as an herbaceous humic brown (10YR 4/3) soil with granular structure with a gradual smooth lower boundary. On the surface, laterally discontinuous concentrations of poorly sorted stone tools eroded from previously intact deposits or episodic from knapping episodes occur along the hillslope, as well as natural deposits of angular to sub-angular cobbles, stones, and boulders.

3.2 Lithostratigraphic Unit 2 – Late Pleistocene Debris Flow.

This deposit represents a continuation of the Holocene debris flow, characterized by poorly sorted brown (7.5YR 5/4) silt loam with many sub-angular to angular cobbles throughout. Deposit is matrix supported, slightly hard, and has weak subangular blocky structure. Deposition of this unit likely began during the transition from the Pleistocene to the Holocene. Lower boundary is clear and wavy.

3.3 Lithostratigraphic Unit 3 – Late Pleistocene Dry Fall.

This deposit represents an increase in depositional energy, marked by angular boulders and a clast-supported matrix of poorly sorted brown (7.5YR 4/4) silt loam. Sediments are slightly hard with subangular blocky structure. Many fine roots throughout. The deposit may represent a dry fall (debris and rock) occurring at the end of the Pleistocene. Lower boundary is abrupt and wavy.

3.4 Lithostratigraphic Unit 4a – 4b – Late Pleistocene Debris flow (Soil 2).

This deposit unconformably underlies the overlying dry fall, and is characterized as a poorly sorted, stony, decalcified strong brown (7.5YR 5/8) sandy loam. The deposit is matrix supported and is pedogenically altered (Bt horizon) as indicated by subangular blocky structure with a hard consistency. These interpretations were confirmed with micromorphology which showed illuvial brown speckled clay coatings with weak striations around sand grains and voids. The deposit was separated into sub-units based on texture sizes, and interpreted to be two colluvial events with varying depositional energy that have been homogenized (pedogenically) by a period of stability occurring between LU4a and LU3. The lower boundary is abrupt and wavy.

3.5 Lithostratigraphic Unit 5 – Aeolian Sand (Last Glacial Maximum - Soil 3).

This deposit is composed of strong brown (7.5YR 5/8) well-rounded loamy sand with common angular to sub-angular cobbles and gravels as inclusions. The frequency of these clasts varies laterally and the deposit thins out down slope. Aeolian sands are post-depositionally altered (Bt horizon) as represented by illuvial reddish brown limpid clay coatings. Lower boundary is abrupt and wavy. This deposit is interpreted as a buried palaeosol (Bt) horizon developed on aeolian sand, the latter perhaps related to sea-level fluctuations and exposure of the donor sediments of the continental shelf by lower sea levels.

3.6 Lithostratigraphic Unit 6 – Late Pleistocene Sandy Mud Flow (Last Interglacial Palaeosol - Soil 4).

This deposit is characterized as a moderately sorted yellowish red (5YR 5/6) to reddish brown (5YR 5/4) sandy clay loam with many gravels throughout. Deposit is a well-developed hard soil with columnar structure with reddish brown clay coating sand grains and infilling pore space as

shown by micromorphology. We suggest the deposit is an aeolian sandy deposit modified by gravity flow processes that had disturbed parts of the underlying layer (see below). Lower boundary is very abrupt and wavy representing an erosional unconformity.

3.7 Lithostratigraphic Unit 7 – Middle Pleistocene Debris Flow (Soil 5).

A very pale brown (10YR 8/4) calcareous sandy loam with many angular cobbles and gravels throughout. Few boulders. Micromorphology demonstrates turbate structures and a heteregenous mixture of calcite and clay with clasts oriented parallel to the general inclination of the layer, the clay component probably inherited from the overlying layer during deposition. Carbonate engulfs and plugs majority of the B horizon (>50% vol. K fabric). Redoximorphic features throughout as non-cemented iron and manganese staining throughout indicating a period of seasonal saturation and subsequent subaerial weathering via water table fluctuation. Lower boundary clear and wavy.

3.8 Lithostratigraphic Unit 8 – Saprolite – Argillically Altered Shale.

A well-sorted deposit of whitish (10YR 8/1) calcareous sandy clay. Concentrations of redoximorphic features include many accumulations of non-cemented iron staining and iron depletions occurring throughout. Minerals are heavily altered and commonly crushed. Deposit represents weathered chert-substrate that has been calcretized (i.e., saprolite).

Supplementary Text

1. Site Formation History

The earliest stratum exposed in trench DG-A/001 is LU8, a non-cultural argillically altered shale deposit (protolith). Micromorphology reveals highly altered minerals and the presence of redoximorphic features as iron (Fe) stains and depletions occurring throughout, indicating the past presence of a locally high (perched) water table with seasonal fluctuation causing subaerial weathering. Capping this deposit is an artefact-bearing pedogenically altered debris flow marked by turbate structures (LU7) dating to MIS 7 (198.4 ± 14.5 ka). The deposit is post-depositionally altered via secondary biogenic calcium carbonate as $CaCO_3$ derived from water leaching carrying Ca^{2+} and HCO_3^- underlying the zone of rooting (phreatic zone) during a warming period (Bkk horizon – S5). The primary source of calcium is most likely windblown (aeolian) calcareous bioclasts from coastal aeolianites. Unconformably overlying and cutting into the calcic horizon is a moderately sorted, clay-rich, sandy mud flow (LU6) with well-developed clay structure (soil formation), dating to the last Interglacial (MIS 5). This Interglacial palaeosol (S4) was heavily eroded, and what is left is a remnant of once a much thicker soil horizon. Today the horizon is 10cm thick and artefact rich (Table 1). This palaeosol is unconformably capped by a deposit of wind-blown sand, deposited as the environment shifted to an aeolian-dominated regime (LU5) dating to 21 – 24 ka or the Last Glacial Maximum (LGM). Following deposition of the sand, a second period of stability occurred, leading to a moderately-developed and rubified palaeosol overlying these sands (Bt horizon - S3). This soil was capped by a mass movement event (colluviation) (LU4b), reflecting a slight decrease in depositional energy (LU4a) around 17-20 ka. A third period of stability occurred, resulting in the rubification of LU4a and LU4b, and a moderately developed and weakly structured palaeosol with subangular-blocky structure (S2). A high energy (rapid) mass movement event (dry fall) capped this deposit, dating from 14-16 ka (LU3). Capping this deposit is a series of colluvial events (massive, non-bedded colluviation) that continued deposition from the Late Pleistocene into the mid-Holocene (LU1 and LU2). A final fifth period of stability is marked by a modern humic soil at the top of LU1 (S1).

2. Lithic Assemblages by Lithostratigraphic Unit

Here, we summarize the techno-typological characteristics of the chipped stone from DG-A/001 from each LU. Full intra-assemblage quantification is provided only for LU2-7, i.e. those where we have scientific dates. As can be expected at a quarry site, each LU contained large quantities of unmodified lithic debris, much of it likely but not demonstrably cultural. Each also contained identifiably cultural material, ranging from ~100 to >2500 pieces per LU, totalling >12000 lithics. Approximately 78% of this material consisted of recognizable blanks (predominantly flakes and blade-like flakes); the remainder consisted of chunks and chips. All technologies were percussion knapped. A minority (~9% of the identifiable cultural material) of this recognizably cultural material was modified/retouched. In addition, approximately 9% of the cultural material is identifiable as diagnostic of specific chronological periods based on techno-typological characteristics and comparability to well-dated material from excavations in continental Greece, Anatolia, and Southwest Asia.

As a result, LUs – whose deposition spans the bulk of the last 200,000 years - may be compared with respect to the total quantity and density of lithics that they contain (Table 1), as well as with respect to the types of blanks present, the proportion of material that is modified and/or diagnostic, and the chronologically diagnostic industries represented.

In the summaries below we consider the assemblage from each LU to contain both lithics contemporary with the sediments and older material. We presume that the bulk of each assemblage – the non-diagnostic material – is a mix of these, but cannot discriminate with any certainty between LU-contemporary and older material. In the case of the diagnostic material, however, we can discriminate basis of the objects' techno-typological characteristics between (i) those parts of the assemblage that are close in date to the colluvium in which they are included, and (ii) artefacts that were already old when deposited. Where lithics are consistent with types notably earlier than the colluvium in which they are found, we consider those to have been resident on the surface for significant time when the colluvium was deposited.

In LU1 there is material consistent in production, form, and modification with Aegean Mesolithic (Early Holocene) assemblages, namely: flake-based and microlithic (sub 2cm), with blanks knapped multi-directionally from larger part-cortical thick flakes and chunks, with a variety of retouched types, commonly denticulates/notches, piercers ('spines'), and scrapers (*27*, *93*).

Products associated with Upper Palaeolithic (Late Pleistocene) traditions of the Aegean are well-represented in LU1-5. Such assemblages, hitherto exclusively documented on the Greek mainland, are primarily blade- and bladelet-based (from bi- and uni-directional cores), with some larger flake-tools, with modified end-products including burins, denticulates, notched pieces, and end-scrapers amongst others (*38, 94*).

A number of assemblages within the sequence also contain artefacts we assign to the Middle Palaeolithic on the basis of their techno-typological characteristics and comparanda from Greek and Anatolian dated sites (*12, 39, 95, 96*). Such assemblages are typified by products from Levallois (flake, blade-like flake, and blade), and discoidal core technologies, with retouched tools including projectiles denticulates, notches, and scrapers; Mousterian tool-types are particularly well-represented in mainland Greece (*12, 39*).

Well-dated Lower Palaeolithic assemblages from Greece and Anatolia are relatively rare. While Acheulean, handaxe/biface-based industries are relatively well documented throughout eastern and central Anatolia (*14, 15*), they were until quite recently poorly known in western Anatolia and Greece until the discovery of Rodafnidia on Lesbos (*40*). The same region has also produced a number of non–Acheulean assemblages of early Middle - Lower Palaeolithic date, typified by thick flakes, blade-like flakes, blades, and chunks, made without preparation and smooth platforms, with retouched forms including denticulates, notches, and scrapers (*12, 40–41, 97, 98*). In the absence of well-dated assemblages of 250-100 100 ka from Greece (*12*), we simply do not have a clear idea what early Middle Palaeolithic material might look like at Stelida. As a result, material that is characteristically pre-Upper Palaeolithic (e.g., thick flakes with unprepared platforms), yet neither 'classically' Middle Palaeolithic (i.e. Levallois or discoidal core products) nor Lower Palaeolithic of the Acheulean tradition, we classify as 'early Middle – Lower Palaeolithic' (i.e. we cannot assign it with confidence to either early Middle or Lower Palaeolithic).

The DG-A/001 assemblages also contain a small quantity of artefacts (n=5) that we assign exclusively to the Lower Palaeolithic (and there are a further 159 finds typologically associated with this period from our surface survey (*25*)), including a biface (fig. S4), denticulate, piercer, and notch.

Although (as can be expected at a quarry site) only a minority of the lithic material can be associated with period-specific lithic industries, the size of the overall sample (Table 1) is such

that the quantities of chronologically diagnostic material are still considerable. We focus below on LU2-LU7, the sealed strata with TAQ dates beginning at 13.8-12.1 ka. Overall patterns are consistent with the dating of these LUs and expectations of lithic industries of these periods. Identifiably Upper Palaeolithic material, which constitutes the majority of the diagnostics, disappears below LU5, where LU6 has a TAQ of 86 ka at the latest. The majority of the identifiably Middle and/or early Middle to Lower Palaeolithic material, conversely, was found in LU6, as should be expected if it were being produced at that time and found only as residual material on the landscape subsequently. This Upper Palaeolithic / pre-Upper Palaeolithic contrast is also notable in the clearly bimodal average size of the lithics (Table 1); this bimodal distribution perhaps suggests that the non-diagnostic material is predominantly derived from the industries associated with the majority of the diagnostics, rather than from residual surface material. The highest estimated densities of material occur in the strata containing Upper Palaeolithic material, suggesting at an increase in intensity of exploitation of Stelida over time.

2.1 Lithostratigraphic Unit 1 - Late Pleistocene to Holocene.

This assemblage of 4607 artefacts, is the only to contain material assigned to the Mesolithic. The modified component includes such typical pieces as those with linear retouch, spines, notches, denticulates, and scrapers. The Upper Palaeolithic tool-types are represented by burins, denticulates, and notched pieces, while a few Levallois cores and flakes, as well as a *déjeté* flake (from a discoidal core), appear to be from the Middle Palaeolithic. That material assigned to the early Middle – Lower Palaeolithic includes a denticulate and side-scraper on larger, thick flakes.

2.2 Lithostratigraphic Unit 2 - Late Pleistocene, TAQ of 13.8-12.1 ka.

This assemblage consists of 1369 chert artefacts, predominantly flakes (71%), chunks (15%), and blade-like flakes (11%); 20% of these were modified. Of the 279 modified pieces, 238 (17% of the LU2 assemblage) were identified as chronologically diagnostic, most of which are assigned to the Upper Palaeolithic (209 pieces, 88% of the diagnostics). The main types of modification in the Upper Palaeolithic assemblage are linear retouch, denticulates, notches, scrapers, and combined tools (together accounting for 90% of this period's retouched material). An early Middle –Lower Palaeolithic component of 29 pieces (12% of the diagnostics) is made

up of flake-based scrapers, denticulates, notches, and combined tools (one a large cutting tool/denticulate/scraper).

2.3 Lithostratigraphic Unit 3 - Late Pleistocene, TAQ of 16.3-14.2 ka.

This assemblage consists of 2468 chert artefacts, predominantly flakes (72%), chunks (19%), and blade-like flakes (6%); 9% of these were modified. Of the 210 modified pieces, 174 (7% of the LU3 assemblage) were identified as chronologically diagnostic. The overwhelming majority of these (157 pieces [90% of the diagnostics]) were identified as Upper Palaeolithic. The retouched component of this Upper Palaeolithic assemblage was made mainly on flakes (56%), blade-like flakes (19%), and blades (18%). Types of retouch include primarily denticulate, linear, notches, scrapers, and combined tools (together comprising 87% of the retouched Upper Palaeolithic assemblage); small numbers of backed pieces, burins, and piercers are also present. There is also a large notched and truncated bipolar blade that can be assigned to the Aurignacian tradition of the earlier Upper Palaeolithic on the basis of its close comparability to well-dated material from mainland Greece and Anatolia (*38, 53, 94, 99*).

Seventeen pieces (11% of the diagnostics) are techno-typologically assigned to the Middle Palaeolithic, including a Mousterian point, as well as Levallois and pseudo-Levallois flakes (fig. S3). The early Middle – Lower Palaeolithic material includes denticulates, scrapers, linear retouched pieces, a notch, a piercer, and a tranchet.

2.4 Lithostratigraphic Unit 4a - 4b - Late Pleistocene, TAQ of 19.7-17.3 ka.

This LU contains a combined total of 2750 chert artefacts, predominantly flakes (71%), chunks (19%), and blade-like flakes (8%); 10% of these were modified. Of the 264 diagnostic pieces (10% of the LU4 assemblage), the overwhelming majority (93%) are considered to be chronologically diagnostic of the Upper Palaeolithic.

The Upper Palaeolithic material consists primarily of flakes (53% of the Upper Palaeolithic assemblage) and blade-like flakes (33%), with a minority component of blades (6%). The modified tools consist of denticulates (23%), pieces with linear retouch (20%), combined tools (13%), scrapers (13%), and notches (11%), with the remainder made up of piercers, burins, and backed pieces. Notable are a double burin on a large blade, as well as two carinated end-

scrapers/bladelet cores and a dihedral burin with lamellar retouch on a large blade, which are diagnostic of the earlier Upper Palaeolithic Aurignacian tradition (*38*, *53*, *94*, *99*) (figs. S2-S3). The early Middle – Lower Palaeolithic component is quite small (n=18, 7% of the diagnostics) and mainly from LU4b (>80%). It consists of a few larger flake-based tools including five denticulates, three linear retouched pieces, two scrapers, and two notches, plus a biface, comparable to examples from dated Aegean Lower Palaeolithic assemblages (fig. S4) (*40*).

2.5 Lithostratigraphic Unit 5 - Last Glacial Maximum, TAQ of 24.2-21.2 ka.

This assemblage consists of 2312 chert artefacts, predominantly flakes (68%), chunks (18%), and blade-like flakes (13%); 11% of these were modified. Of the 257 chronologically diagnostic pieces (11% of the LU5 assemblage), the majority (72%) are considered to be typical of the Upper Palaeolithic.

The Upper Palaeolithic material consists primarily of flakes (51% of the Upper Palaeolithic assemblage) and blade-like flakes (30%), with a minority component of chunks (10%) and blades (8%). The most common types of modification are denticulates (32%), followed by linear retouch (17%), scrapers (15%), combined tools (10%), and burins (9%), as well as notches, piercers, and backed pieces.

The most common early Middle – Lower Palaeolithic diagnostics (n=73, 28% of the diagnostics) are denticulates (37%), followed by scrapers (15%), pieces with linear retouch (15%), and combined tools (12%), as well as notches and a pick.

2.6 Lithostratigraphic Unit 6 - Late Pleistocene, Last Interglacial, TAQ of 100.1-86 ka.

The 548 chert artefacts from LU6 consist primarily of flakes (66%), blade-like flakes (14%), and chunks (13%); 9% of these were modified. Although only 9% of the blanks were retouched, 26% of the assemblage, clear products of technologies associated with Middle and/or early Middle to Lower Palaeolithic assemblages of Greece/Anatolia (see above), is considered chronologically diagnostic. While this component includes three unmodified blanks from Middle Palaeolithic Levallois and pseudo-Levallois traditions, the vast majority of the diagnostic material (95%) is assigned to the early Middle – Lower Palaeolithic. This material includes flakes (59%) and blade-like flakes (15%), with a minority (36%) of modified pieces including denticulates (22% of modified pieces, including one convergent, a ‘Tayac point’) and notches (22%), as well as

pieces with linear retouch (16%), scrapers (14%), combined tools (12%), and piercers, burins, and a tranchet (14% combined) (Fig. 3).

2.7 Lithostratigraphic Unit 7 - Middle Pleistocene, TAQ of 219.9-189.3 ka.

LU 7 contained a relatively small assemblage of 106 pieces, consisting primarily of flakes (74%) with minor components of chunks and blade-like flakes. Only three recognisably modified pieces, two denticulates and a scraper, were found; none are chronologically diagnostic, but are dated to the early Middle – Lower Palaeolithic on the basis of the stratum's TAQ (Fig. 3).

2.8 Lithostratigraphic Unit 8.

No cultural material was recovered from the ~0.5 m^3 of sediment that was excavated and screened.

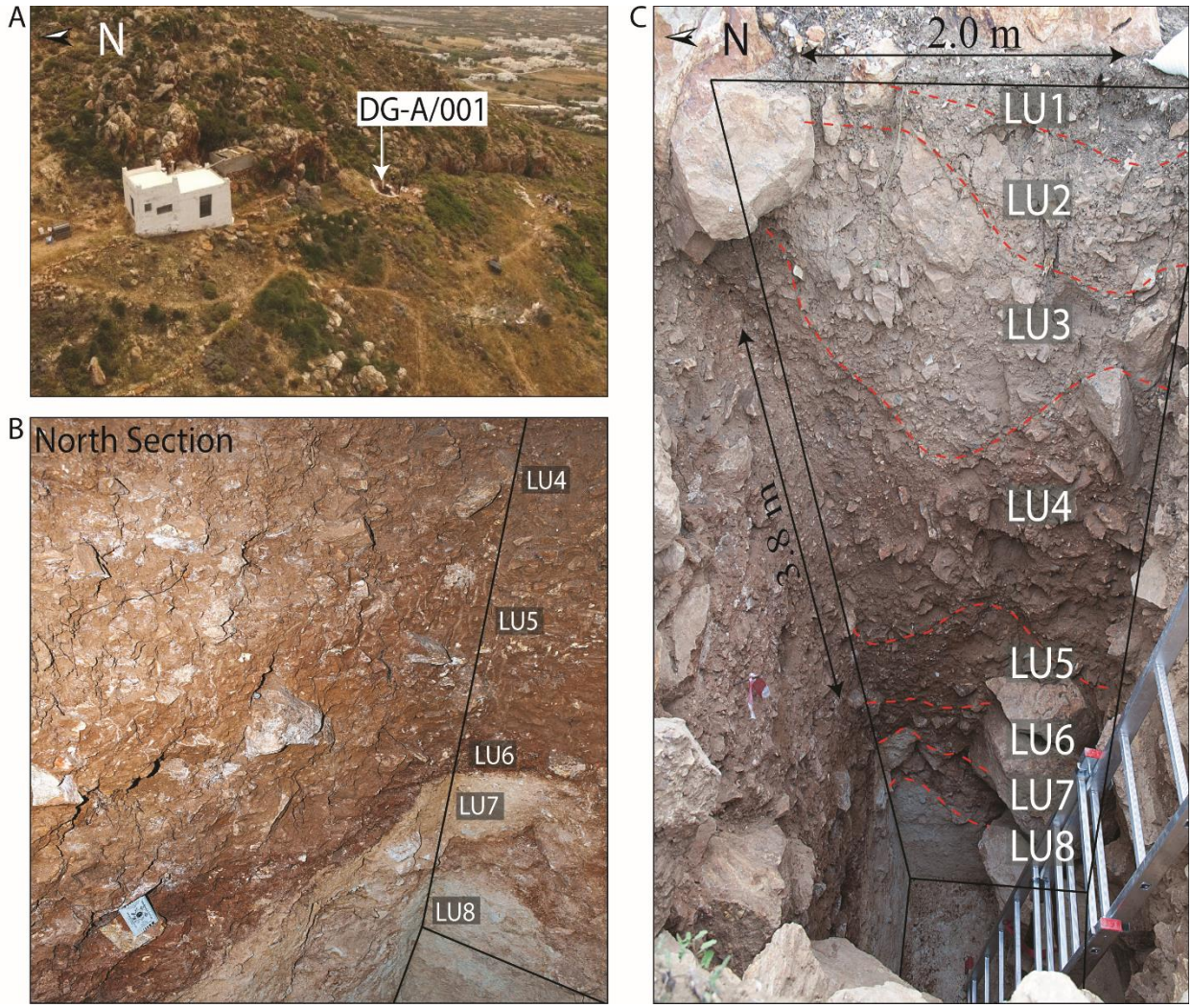

Fig. S1. Geomorphic context of excavation unit DG-A/001. (A) Location of excavation unit DG-A/001 on the Stelida hillslope. **(B)** Pedogenically altered and stratified debris and mudflows at the bottom of excavation unit DG-A/001. **(C)** Fully excavated section of unit DG-A/001 with stratigraphic boundaries outlined by red dashed lines. J. Holcomb and P. Karkanas.

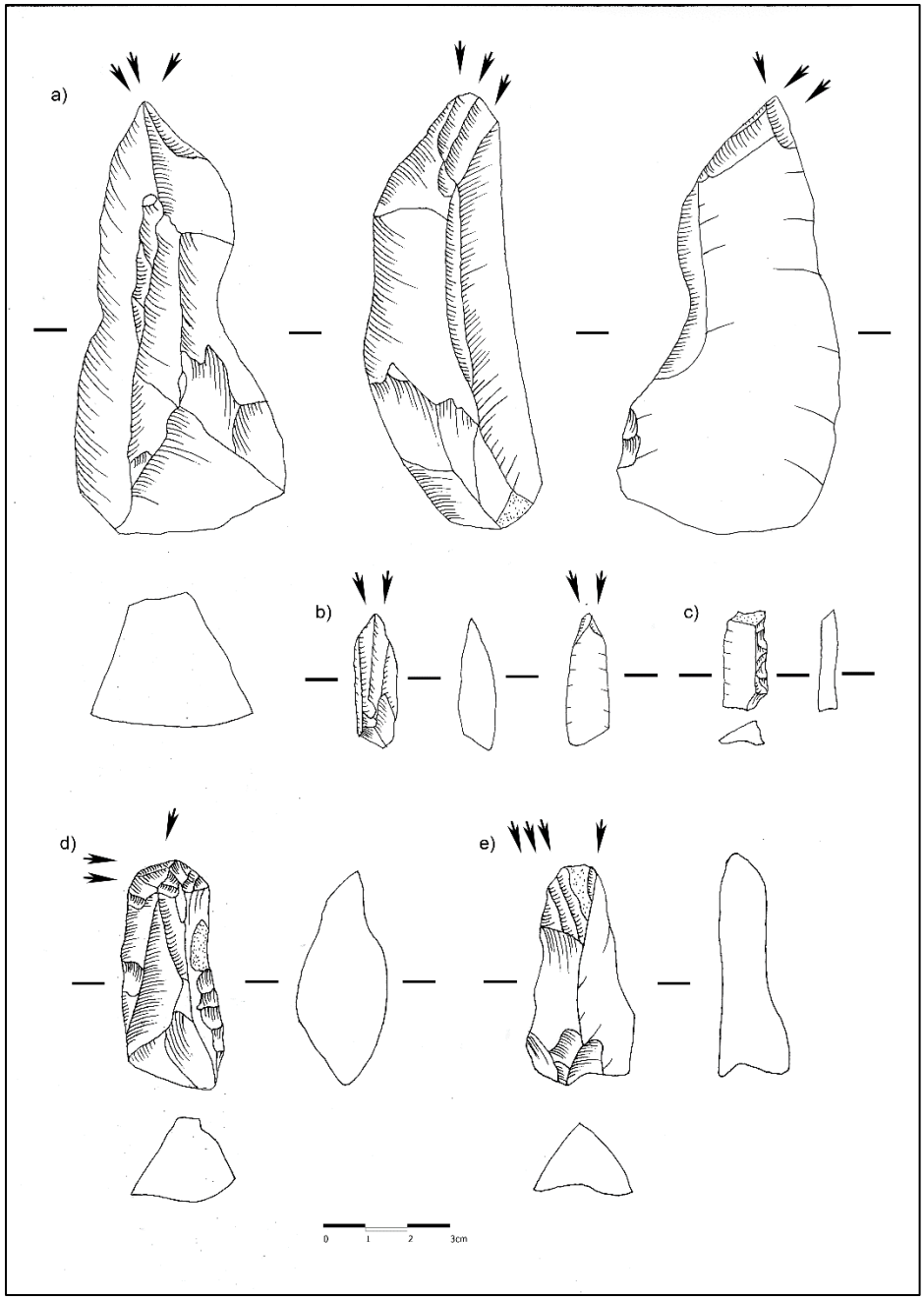

Fig. S2. Select Upper Paleolithic diagnostic artifacts from LU3 to LU5. Select Upper Palaeolithic diagnostic artefacts from lithostratigraphic units [LU] 3-5; **a,** dihedral burin on core (LU4a), **b,** dihedral burin on blade (LU5), **c,** backed blade (LU3), **d,** transversal burin on a core (LU4b), **e,** carinated scraper / bladelet core (LU4b). D.D. Mihailović.

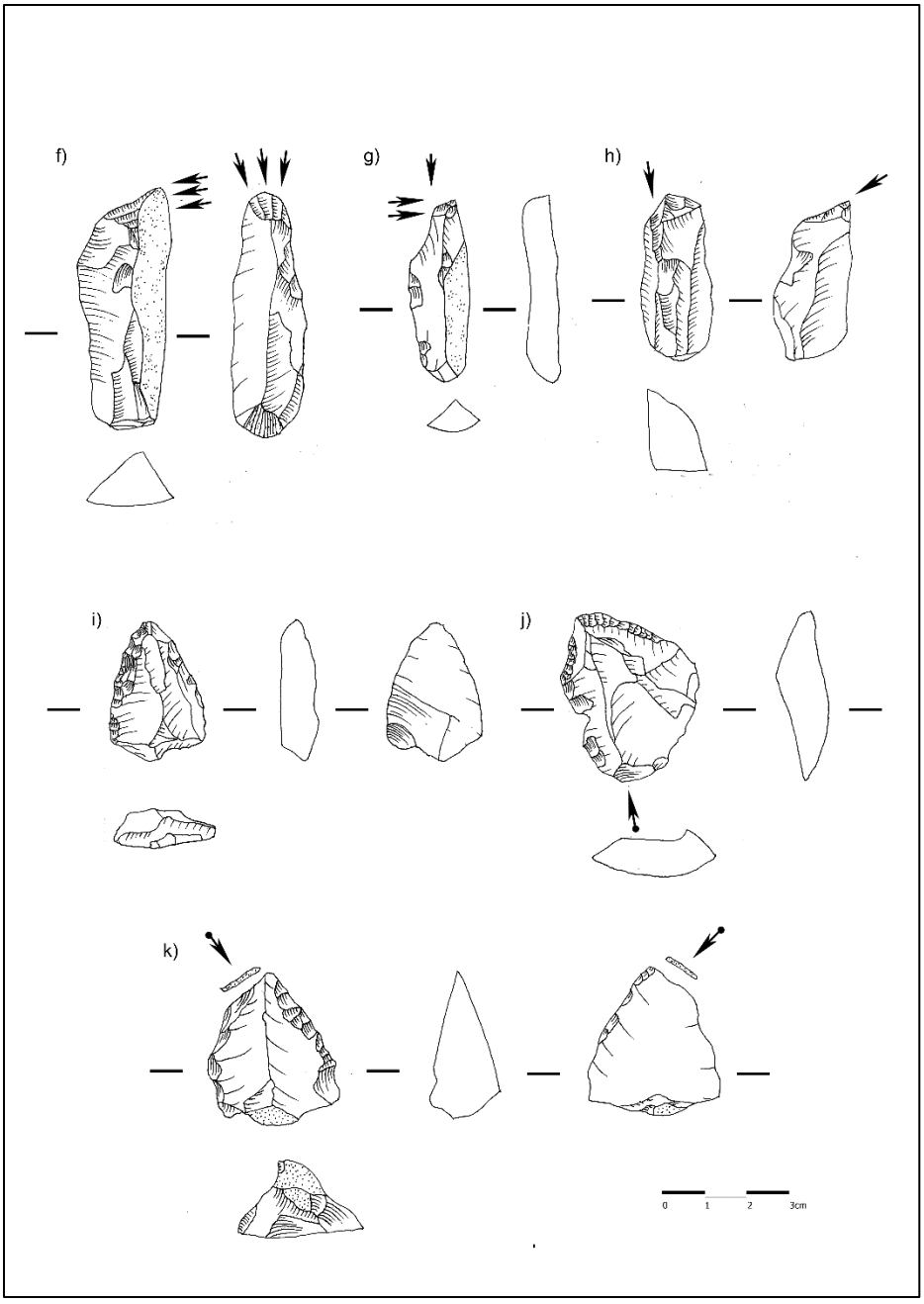

Fig. S3. Select Upper and Middle Paleolithic diagnostic artifacts from LU2 to LU5. Select Upper and Middle Palaeolithic diagnostic artefacts from lithostratigraphic units [LU] 2-5; **f,** carinated scraper / bladelet core (LU2), **g,** transversal/lateral burin on blade (LU4a), **h,** mesial burin on core (LU5), **i,** Mousterian point (LU3), **j,** Pseudo-Levallois point (LU3), **k,** convergent scraper on flake (LU3). D.D. Mihailović.

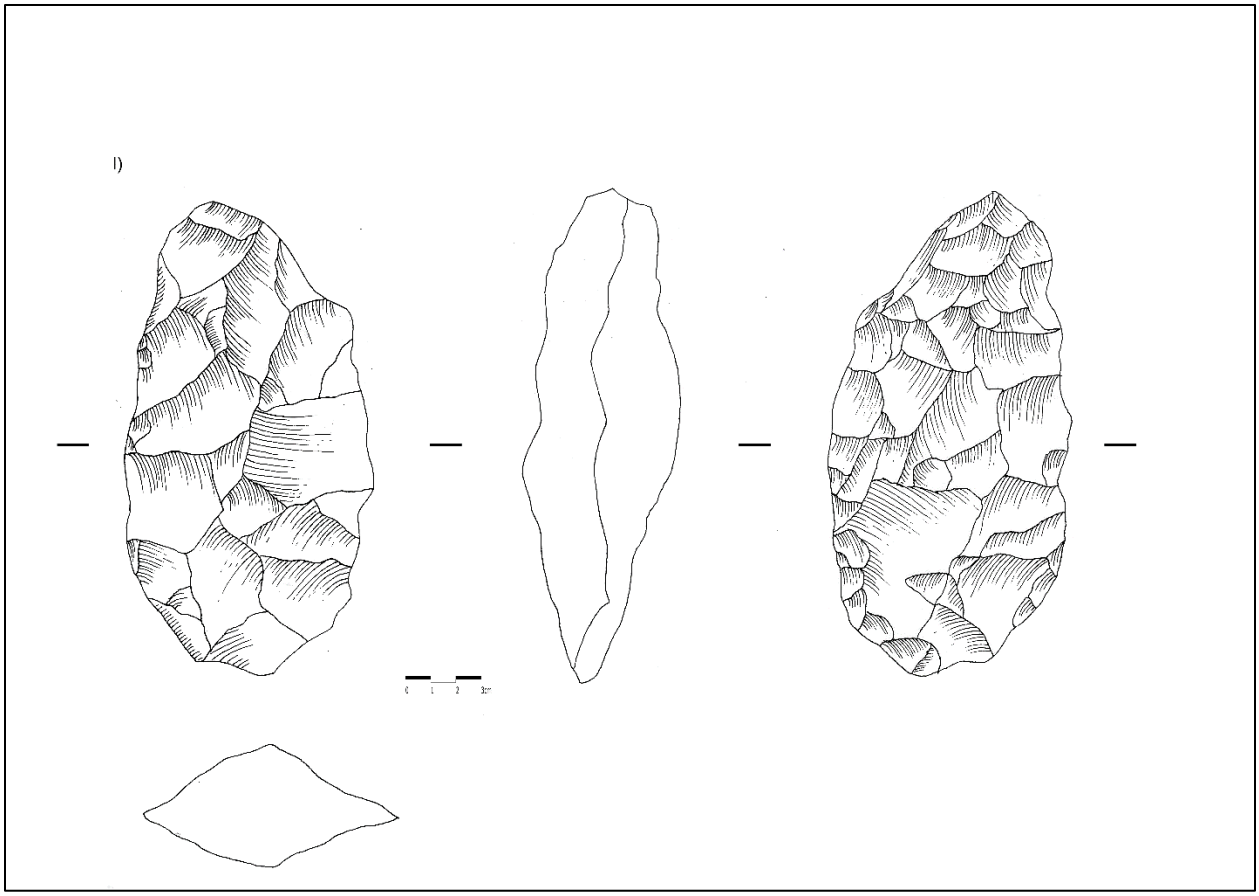

Fig. S4. Lower Paleolithic biface (LU4b). D.D. Mihailović.

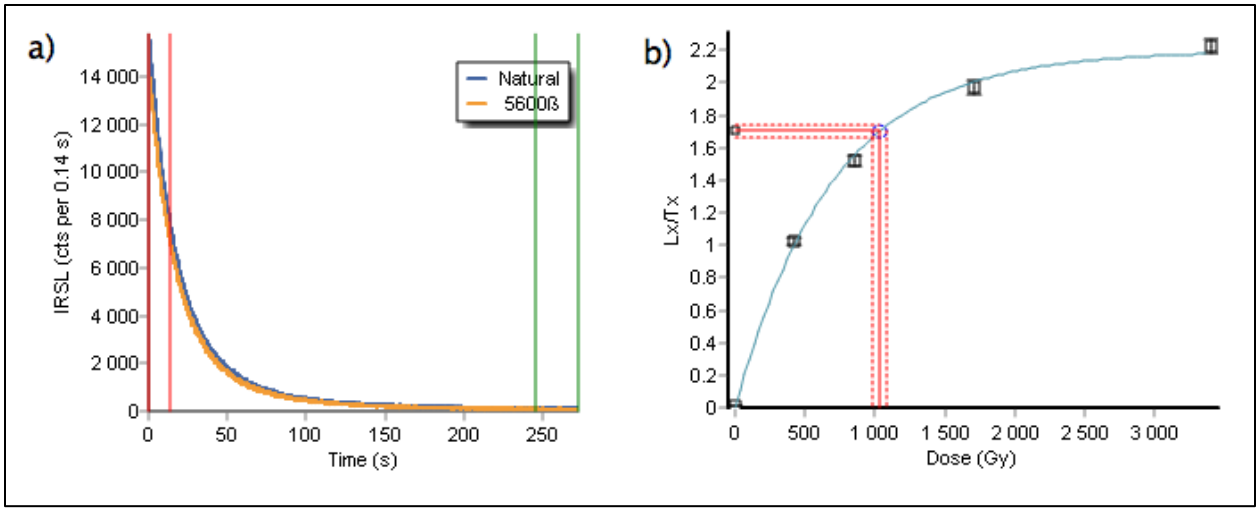

Fig. S5. $pIRIR_{290}$ typical shine-down curve (a) and dose response curve (b) for sample SNPA17-04. C. Lahaye.

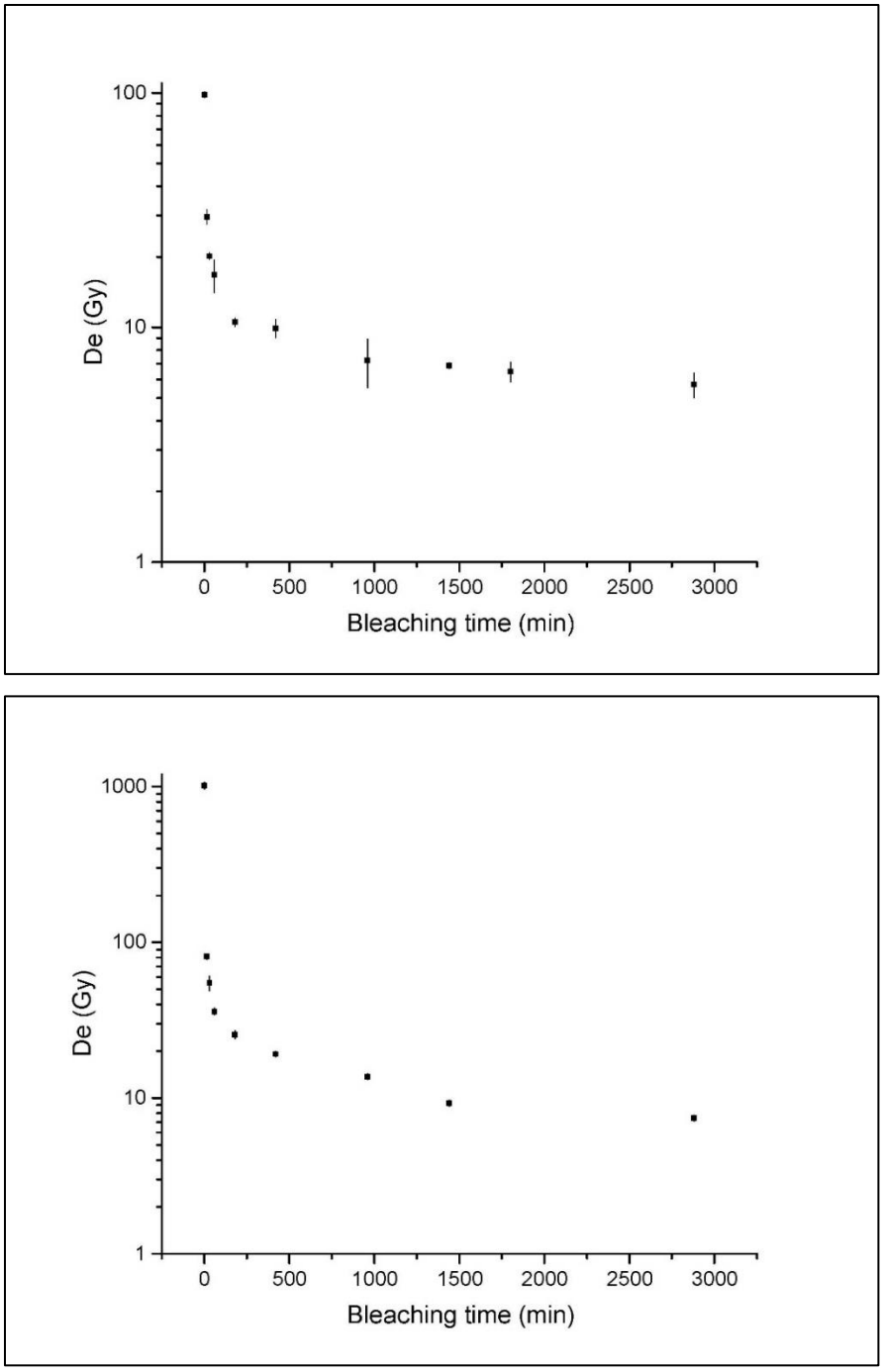

Fig. S6. Residual dose measurements as a function of time, after 15 min to 48 hours of light exposition in a solar simulator, for sample SNAP16-02 (top) and SNAP17-04 (bottom). N. Taffin and C. Lahaye.

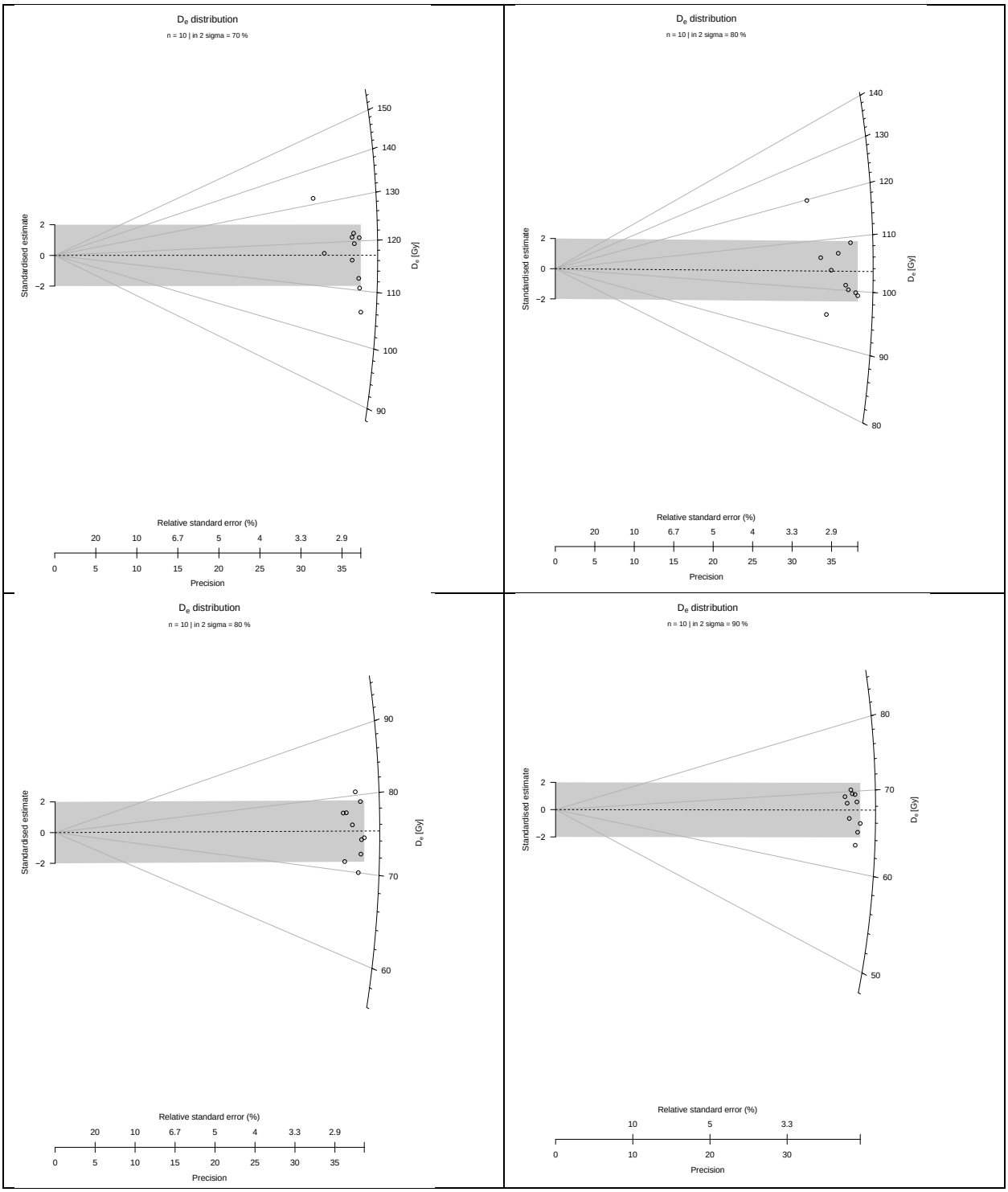
De distribution
n = 10 | in 2 sigma = 70 %
Standardised estimate
De [Gy]
Relative standard error (%)
Precision
De distribution
n = 10 | in 2 sigma = 80 %
Standardised estimate
De [Gy]
Relative standard error (%)
Precision
De distribution
n = 10 | in 2 sigma = 80 %
Standardised estimate
De [Gy]
Relative standard error (%)
Precision
De distribution
n = 10 | in 2 sigma = 90 %
Standardised estimate
De [Gy]
Relative standard error (%)
Precision

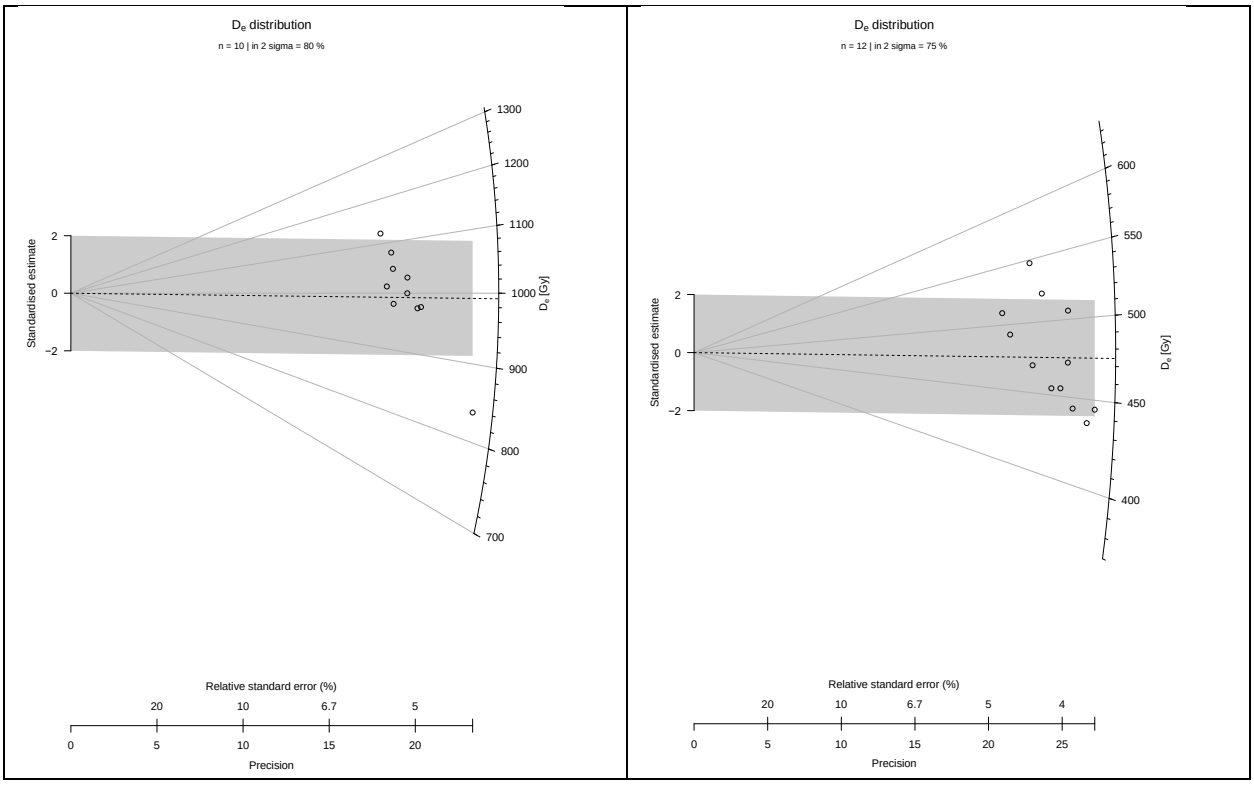

Fig. S7. Radial plots of the pIR-IR_{290} measurements for: SNAP16-01 (top left); SNAP16-02 (top right); SNAP16-03 (middle left); SNAP16-04 (middle right); SNAP17-04 (bottom left); SNAP17-05 (bottom right).

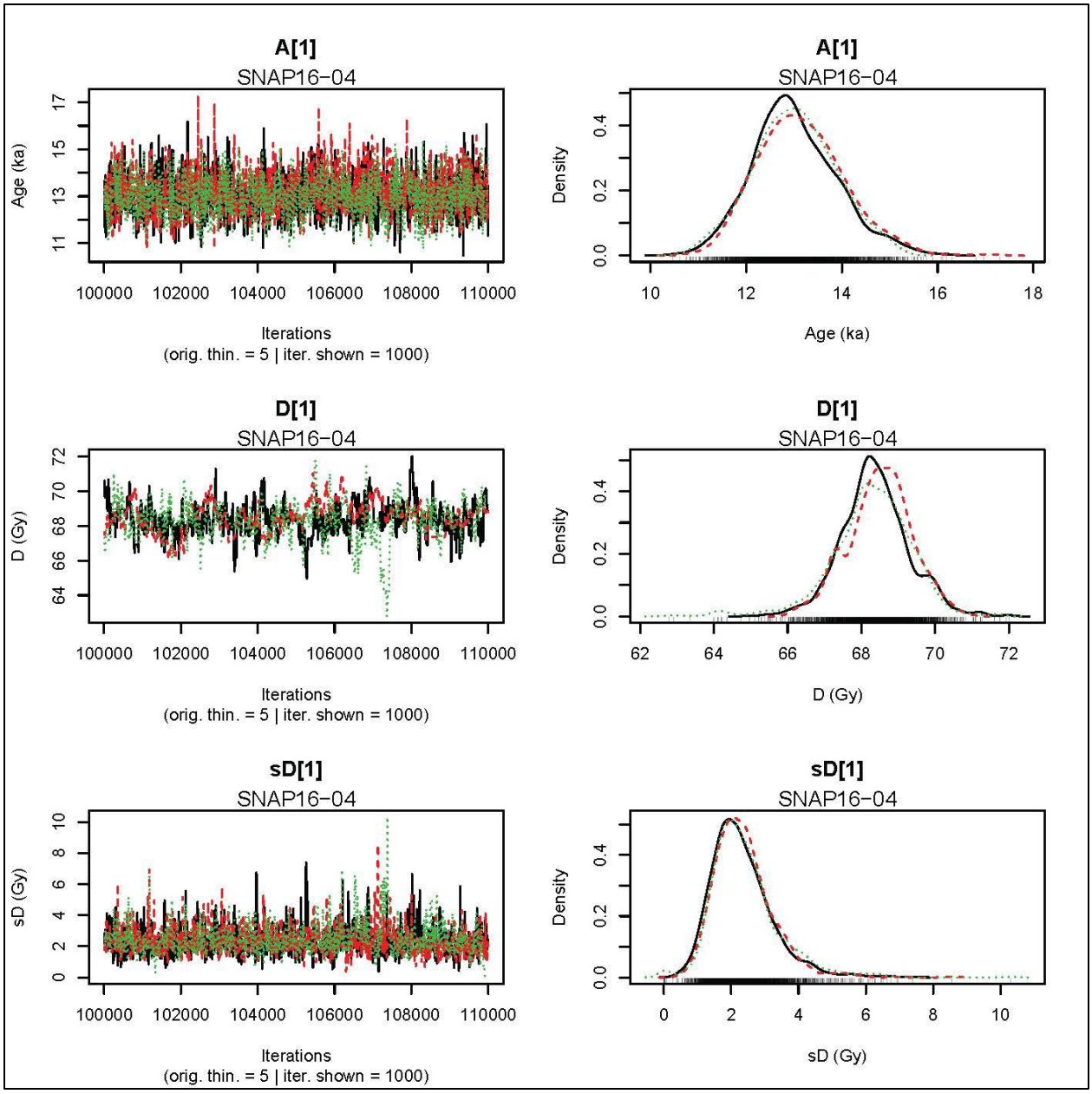

Fig. S8. Output of the Markov Chain Monte Carlo calculations for the $pIRIR_{290}$ age (top row), palaeodose (middle row), and dispersion of equivalent doses (bottom row) of sample SNAP16-4, as generated by the R 'BayLum' package. A good convergence of the Markov Chains is reached after 50,000 chains. G. Guérin.

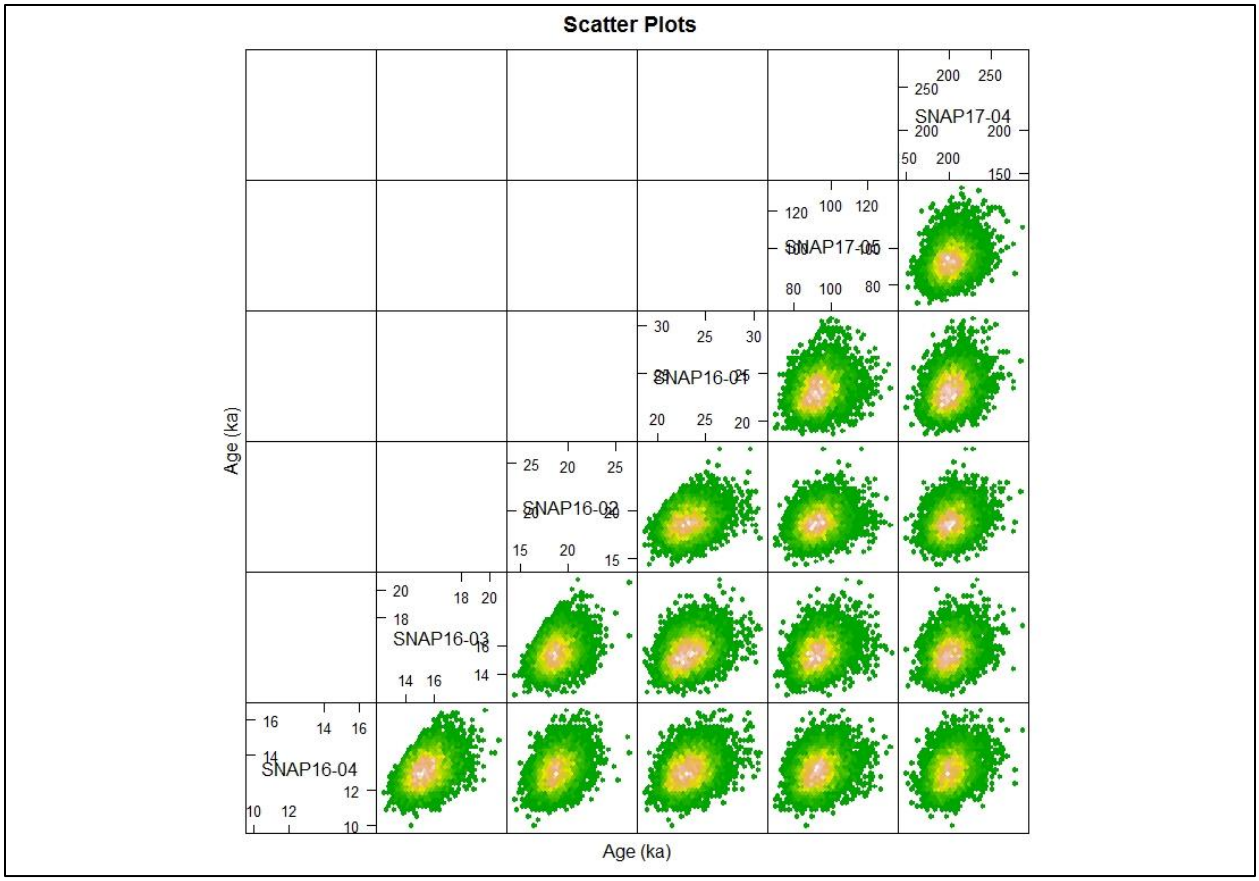

Fig. S9. Bivariate scatterplot of a sample of observations from the joint posterior distribution of the IRSL ages generated by Markov Chain Monte Carlo calculations, using the "BayLum" R package. G. Guérin.

Table S1. Main characteristics of the $pIRIR_{290}$ ages measurements for the DG-A/001 stratigraphic sequence. Equivalent doses ('D_e') obtained with the Average Dose Model ('ADM') and Central Age Model ('CAM'), from $pIRIR_{290}$ measurements. The overdispersion ('OD') values were determined with the Central Age Model. D_e and total dose rates with statistics uncertainties, and ages at 1σ (total uncertainty). The '**Age BayLum model (ka)**' column gives the 68% C.I. for the age of each sample as modelled with the BayLum package.

Sample ID.	Context	D_e (Gy) ADM	D_e (Gy) CAM	OD (CAM)	Total dose rate ($Gy.ka^{-1}$)	Age ADM (ka)	Age BayLum model (ka)
SNAP-16-4	LU2	68±1	68±1	2±1%	5.27±0.06	12.9±0.9	13.8-12.1
SNAP-16-3	LU3	75±1	75±1	4±1%	5.03±0.09	14.9±1.0	16.3-14.2
SNAP-16-2	LU4b	104±2	104±2	5±2%	5.71±0.11	18.2±1.3	19.7-17.3
SNAP-16-1	LU5	117±2	117±2	5±2%	5.30±0.05	22.1±1.5	24.2-21.2
SNAP-17-5	LU6	478±10	477±10	6±2%	5.07±0.06	94.1±6.5	100.1-86.0
SNAP-17-4	LU7	1000±24	999±25	6±2%	5.03±0.11	198.4±14.5	219.9-189.3

Table S2. Main characteristics of the IR_{50} age measurements. 'LU': lithostratigraphic unit. '$g_{2\text{-days}}$': laboratory fading rate (*56*). 'D_e (Gy) IR_{50} uncorr.' corresponds to the uncorrected equivalent dose (and associated statistical uncertainty) measured with the IR_{50}. The DRC correction method was applied to correct for fading (*71*) and the age uncertainties include a 2% uncertainty of the laboratory source dose rate.

Sample ID.	LU	$g_{2\text{-days}}$ (% decade)	D_e (Gy) IR_{50} uncorr.	Age IR_{50} corr. DRC (ka)
SNAP-16-4	2	4.4±0.8	35.0±3.1	12.1±1.2
SNAP-16-3	3	4.1±0.4	42.3±4.5	15.0±1.8
SNAP-16-2	4b	4.3±1.2	53.1±6.5	17.4±2.6
SNAP-16-1	5	3.4±0.3	61.1±1.8	18.5±0.7

Table S3. Radioelements contents determined by high-resolution gamma spectrometry.

Radioelements contents determined by high-resolution gamma spectrometry (LU = lithostratigraphic unit).

Sample ID.	LU	K (%)	U (^{226}Ra) (ppm)	Th (ppm)
SNAP-16-4	2	2.56±0.03	4.64±0.04	26.58±0.18
SNAP-16-3	3	2.60±0.03	4.90±0.04	25.46±0.18
SNAP-16-2	4b	2.30±0.03	5.24±0.04	28.28±0.20
SNAP-16-1	5	2.62±0.03	4.01±0.03	22.12±0.16
SNAP-17-5	6	2.52±0.03	4.58±0.04	25.29±0.19
SNAP-17-4	7	2.72±0.03	2.77±0.03	22.62±0.17

Table S4. IR_{50} and $pIRIR_{290}$ dose-rate information. Etching was taken into account for the beta dose-rates when necessary. 'LU': lithostratigraphic unit.

Sample ID.	LU	Internal Dose rate ($Gy.ka^{-1}$)	External dose rate (alpha+beta+gamma+cosm) ($Gy.ka^{-1}$)	Envir. Dose rate (gamma+cosmic) ($Gy.ka^{-1}$)	Total dose rate ($Gy.ka^{-1}$)
SNAP-16-4	2	0.76±0.03	4.51±0.05	1.63±0.04	5.27±0.06
SNAP-16-3	3	0.76±0.03	4.27±0.09	1.35±0.08	5.03±0.09
SNAP-16-2	4b	0.76±0.03	4.96±0.10	2.13±0.10	5.71±0.11
SNAP-16-1	5	0.76±0.03	4.54±0.04	1.80±0.02	5.30±0.05
SNAP-17-5	6	0.79±0.03	4.28±0.05	1.64±0.05	5.07±0.06
SNAP-17-4	7	0.79±0.03	4.24±0.11	1.72±0.11	5.03±0.11